Inhibited emission of electromagnetic modes confined in subwavelength cavities

N. Le Thomas and R. Houdré
Institut de Physique de la Matière Condensée, École Polytechnique Fédérale de Lausanne (EPFL), Station 3, CH-1015 Lausanne, Switzerland
(Received 20 May 2011; published 27 July 2011)

We experimentally demonstrate the active inhibition of subwavelength confined cavity modes emission and quality factor enhancement by controlling the cavity optical surrounding. The intrinsic radiation angular spectrum of modes confined in planar photonics crystal cavities as well as its modifications depending on the environment are inferred via a transfer matrix modeling and k-space imaging.

DOI: 10.1103/PhysRevB.84.035320 PACS number(s): 42.70.Qs, 12.20.−m, 42.30.Kq, 42.60.Da

I. INTRODUCTION

Since the prediction by Purcell in 1946 that the rate of spontaneous emission γ_{sp} of a dipole can be modified with a resonant cavity,[1] this effect has been observed with a large variety of emitters such as atom,[2] molecules,[3–5] or semiconductor heterostructures.[6–8] According to the Fermi's golden rule, the rate of dipole spontaneous emission is given by $\gamma_{sp}(\vec{k},\sigma;\omega_k) = \frac{2\pi}{\hbar}|\hat{d}\cdot\hat{E}^{+}_{\vec{k},\sigma}|^2\rho(\vec{k},\sigma;\omega_k)$, where ρ is the density of state of the electromagnetic vacuum field for a frequency ω_k, wave vector $\vec{k}$ and polarization σ, $\hat{E}^{+}_{\vec{k},\sigma}$ is the electric field creation operator at the dipole, and $\hat{d}$ the dipole operator. The density of state ρ depends on the size and on the dimensionality of the cavity,[9,10] whereas the field amplitude at the location of the dipole is governed by interference or screening effects.[6]

In this paper, we apply such concept of spontaneous emission modification to a new class of emitters formed by electromagnetic modes confined in photonic cavities. The rate of radiation losses γ_{rad} of confined modes can be treated with a perturbative approach similar to the Fermi's golden rule.[11,12] The induced polarization of the mode inside the resonant cavity plays the role of the dipole moment. The dipolar coupling term $\hat{d}\cdot\hat{E}^{+}_{\vec{k},\sigma}$ is substituted for an overlap integral between the fields of the confined mode and the leaky modes of the cavity, while ρ is replaced by the density of state of the cavity leaky modes. As a result, inhibition or enhancement of the confined mode emission is expected depending on the environment, in a similar way to the dipole emission. In particular, we demonstrate here that a planar reflector in the neighborhood of the confined mode can enhance the cavity quality factor Q by canceling the magnitude of the cavity leaky modes. Such a phenomenon relies on interference effects that are revealed in the far field.

II. EXPERIMENTAL METHODS

To identify the nature of the optical surrounding perturbation on a confined mode, we measure both the angular spectrum of the emission[13] and the quality factor Q. The angular spectrum of the field, which results from the decomposition of the field into plane wave, provides a direct access to the modal loss channels. The radiative part of the angular spectrum, i.e., the waves that can propagate in free space, is experimentally accessible with far-field optics as shown in Fig. 1. The resulting experimental far-field pattern is represented in k-space, where one particular point is associated with one direction of emission and gives the weight of the corresponding plane wave in the decomposition of the field.

Among the different types of subwavelength cavities, planar dielectric photonic crystal (PhC) cavities defined in membranes of subwavelength scale thickness (see Fig. 1) can combine the advantage of a large Q factor with a strong confinement of the electromagnetic mode in a volume smaller than the wavelength cube.[14,15] Here, we focus, as a model system, on a so-called L3 photonic crystal cavities to highlight the Q factor enhancement induced by a decrease in the field amplitude of the leaky modes. These cavities are defined by a line defect of three missing holes inside a triangular lattice of holes (lattice constant $a = 460$ nm) etched in a 220 nm thick silicon membrane. They were patterned with deep UV lithography on silicon on insulator (SOI) wafer and designed to operate at a wavelength around 1.55 μm. The light coupling into the cavity mode is carried out via a side coupled W1 photonic crystal waveguide defined by a single line of missing holes and located three lines of holes away from the cavity [see Fig. 1(a)].

The measured cavity Q factor for the L3 cavity investigated in Fig. 1 is 450 before and 3700 after removal of the buried 2 μm thick oxide (BOX). For such measured values of Q, the silicon absorption effect is negligible. The Q factor can be split into three contributions: $1/Q = 1/Q_H + 1/Q_V + 1/Q_C$, where Q_H, Q_V, and Q_C correspond to the in-plane, the out-of-plane and the coupling losses, respectively. The efficiency of the photonic band gap is such that the optical leakage through the PhC barriers are also negligible. The main contribution to the in-plane losses is the coupling loss via the W1 access waveguide. From the light transmission through the W1 access waveguide, we estimate $Q_C \simeq 12\,000$. The out-of-plane contribution Q_V results from the radiative coupling to the far field and from the evanescent coupling with the environment. We mainly focus here on the radiative coupling contribution and its modification via multiple interference effects.

The far-field angular spectrum of the confined mode is directly measured in the back focal plane of a high numerical aperture (NA = 0.95) microscope objective as described in Ref. 16. The high numerical aperture of the microscope objective allows us to probe 90% of the light cone (continuous red/gray circle) as shown in Figs. 1(b) and 1(c) for the fundamental mode of a standard L3 cavity. The light cone

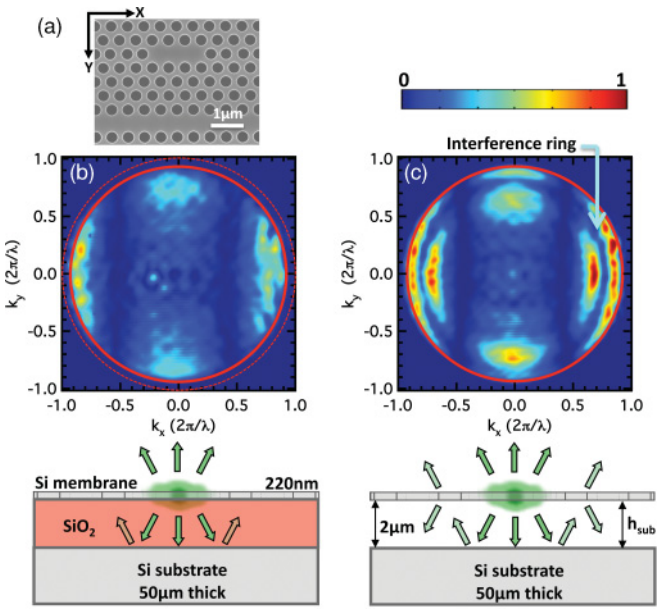

FIG. 1. (Color online) (a) Scanning electron micrograph of a typical silicon L3 cavity coupled to a W1 photonic crystal waveguide. (b) and (c) Experimental far-field angular spectrum of the confined mode of a L3 cavity, on silicon oxide and without silicon oxide, respectively.

is the spatial frequencies domain whose corresponding waves can propagate in free space. For an angular frequency ω_0, the light cone (dashed circle) is defined by $k_x^2 + k_y^2 \leqslant (\omega_0/c)^2$, where k_x and k_y are the components of the in-plane spatial frequency of the field with k_x oriented here along the cavity line defect, and c is the speed of light. The missing 10% of the radiative contribution of the angular spectrum can be inferred via analytical continuation.[16]

Figure 1 reveals the impact of the optical surrounding on the angular spectrum of the confined mode. The field emission is collected from the top surface side of the Si membrane before [Fig. 1(b)] and after [Fig. 1(c)] the BOX is wet etched. In both cases, the cavity in-plane mode profile is approximatively the same, even if there is a slight perturbative change of the waveguide effective index and more losses into the BOX layer due to a larger radiative cone. This similarity is confirmed by the same overall envelope of the intensity distribution of the far-field angular spectrum in both cases. However, as a main difference, a destructive interference ring takes place for the free standing membrane, which comes from the reflection at the interface between the air and the Si substrate as described below.

III. THEORY

The results of the multiple interference effect induced by the optical surrounding of the cavity can be modeled accurately with the transfer matrix T of the optical environment.[17–19] Such a modeling relies on the transverse electric field continuity at each layer interfaces and on the linearity of the scattering problem that allows the plane wave decomposition of the field in the spatial frequency space. The angular spectrum of the cavity mode is split into two source terms: a contribution that radiates above the membrane $E_s^+(k_x,k_y)$ and a contribution that radiates below the membrane $E_s^-(k_x,k_y)$, for each mode (k_x,k_y). With the assumption that the holes of the photonic crystal layer are perfectly vertical, the symmetry of the membrane implies $E_s^-(k_x,k_y) = E_s^+(k_x,k_y) = \frac{E_{\text{cav}}(k_x,k_y)}{2}$, where E_{cav} is the field of the cavity mode. The transfer matrices for E_s^+ and E_s^- are determined from the Fresnel relations at each interface for each mode. The multiple interference process in the PhC membrane are accounted via its effective index value of $n = 3.2$.[20] In the present case, the fundamental cavity mode is TE polarized, i.e., the electric field is parallel to the membrane layer. In addition, the radiated electric field is mainly oriented along the y direction in the far field as experimentally verified over the entire radiative part of the k-space. As a result, only the p polarized Fresnel coefficients are considered for the modes $(k_x,k_y = 0)$ and only the s polarized ones for the modes $(k_x = 0,k_y)$. For all modes (k_x,k_y), the intensity measured in k-space is given by $I_{\text{mes}}(k_x,k_y) = |t(k_x,k_y)|^2 \cdot I_{\text{cav}}(k_x,k_y)$, where $t(k_x,k_y)$ is the amplitude transfer function and $I_{\text{cav}}(k_x,k_y)$ is the radiative angular spectrum intensity when the PhC membrane is considered in vacuum, i.e., from surrounding layers. The transfer function $t(k_x,k_y)$ that depends on the elements of T can be separated into a p contribution $t_p(k_x,k_y)$ and an s contribution $t_s(k_x,k_y)$ according to: $|t(k_x,k_y)|^2 = \frac{1}{4}((|t_p(k_x,k_y)| \cdot k_x/k_r)^2 + (|t_s(k_x,k_y)| \cdot k_y/k_r)^2)$, with $k_r = (k_x^2 + k_y^2)^{1/2}$.

The intensity transfer function $|t(k_x,k_y)|^2$ corresponding to the cases with [Fig. 1(b)] and without [Fig. 1(c)] buried silicon oxide are represented in Figs. 2(a) and 2(b), respectively. It follows that the interference ring visible in Fig. 1(c) is in agreement with the theoretical transfer function in Fig. 2(b). It is not observed in Fig. 1(b) because of the larger value of the buried silicon oxide ($n_{\text{BOX}} = 1.44$) compared to the index of

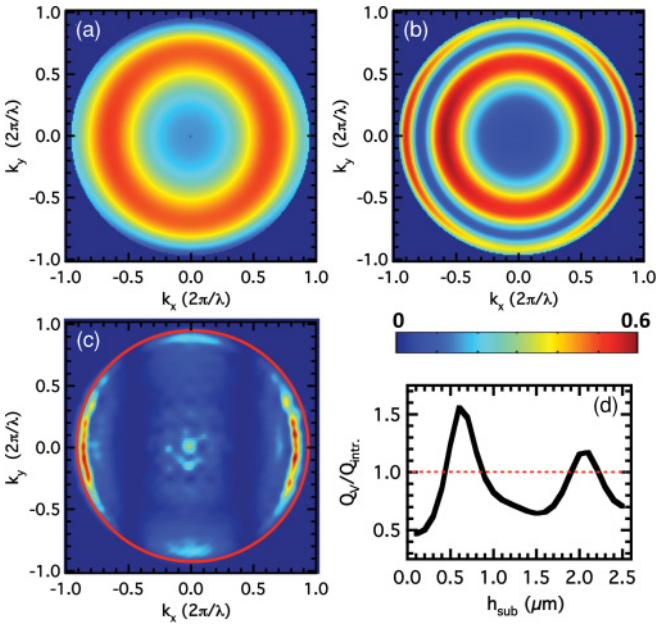

FIG. 2. (Color online) (a) and (b) Theoretical far-field transfer function map $|t(k_x,k_y)|^2$ corresponding to Figs. 1(b) and 1(c), respectively. (c) Intensity angular spectrum of a L3 cavity in vacuum. (d) Theoretical variations of the radiative quality factor induced by a Si reflector for a L3 cavity, normalized to its intrinsic value, $Q_{\text{intr.}}$ (i.e., substrate at infinity).

air, as can be seen in Fig. 2(a). The measured far-field angular spectra $I_{mes}(k_x,k_y)$ and the theoretical transfer function give access to radiative angular spectrum intensity I_{cav} of the cavity free from any surrounding layers except vacuum, as shown in Fig. 2(c). A tiny signature of the interference ring is still present in the reconstructed pattern I_{cav} due to the discretization of the experimental images.

From the reconstruction of I_{cav}, such as the patterns in Fig. 2(c), the impact of any arbitrary surrounding multilayer stacks on the far-field emission pattern can be predicted. As the radiation loss rate is proportional to the total radiated intensity, the variation of the radiative quality factor Q_V can be determined as well for any arbitrary multilayer stacks. In particular, the knowledge of the 2D map $|t(k_x,k_y)|^2$ allows us to determine the evolution of the radiative quality factor Q_V versus the distance h_{sub} [see Fig. 2(d)]. Two maxima are observed in Fig. 2(d), one at $h_{sub} = 0.6$ μm and the other at $h_{sub} = 2.1$ μm. Similar theoretical impact of the substrate on the radiation losses for different PhC structures was already pointed out in Refs. 21–23. The impact of the evanescent coupling with the substrate and the coupling between TE and TM polarized modes, which are not considered by the current model, are negligible for $h_{sub} > 0.5$ μm and the current values of the cavity Q factor ($Q < 2 \times 10^4$).[21]

Four main effects can contribute to lower the Q factor with the presence of the oxide layer: (1) the modes that can propagate into the oxide layer, i.e., whose spatial frequencies satisfy $(\omega_0/c)^2 \leqslant k_x^2 + k_y^2 \leqslant n_{BOX}^2(\omega_0/c)^2$, constitute a significant intensity loss channel, (2) the modes, whose angular spectrum is located outside the BOX radiative cone can be more efficiently evanescently coupled into the Si substrate than in the case of an air spacing layer due to reduction of the vertical modal confinement, (3) the multiple interference effects are less favorable in the far field due to lower index contrast, (4) the vertical asymmetry of the structure can induce in-plane losses via TE/TM modes coupling.[24] Based on the far-field modeling described above, the measured Q factor is expected to reach 2150 if only the multiple interference effect is taken into account, which contrasts with the actual value of 450.

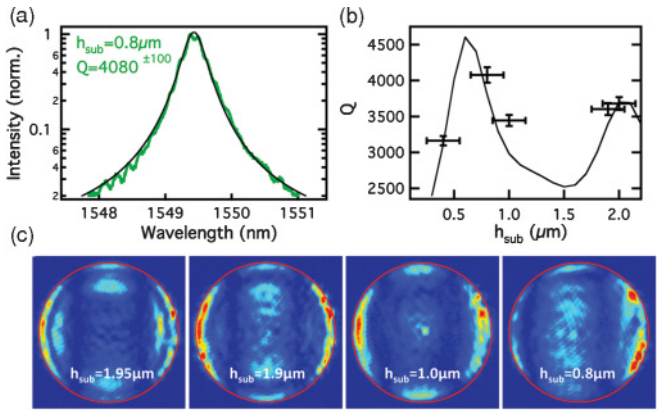

FIG. 3. (Color online) (a) L3 cavity mode spectrum (green/gray curve) for a substrate/PhC slab spacing $h_{sub} = 0.8$ μm with the corresponding Lorentzian fit (thin dark line). (b) Experimental (dot with error bars) and theoretical (line) variation of the L3 cavity factor versus h_{sub}. (c) Evolution of the far-field angular spectrum versus h_{sub} (red/gray circle: NA = 0.95).

The multiple interference effect has a marginal impact in this configuration. As a result, the cavity Q factor has to be limited by free space losses to take advantage of such an effect. With Figs. 3 and 5, we describe two cases in the following where the Q factor is mainly determined by the multiple interference effects.

IV. EXPERIMENTAL DEMONSTRATION OF CAVITY Q FACTOR CONTROL VIA THE MULTIPLE INTERFERENCE EFFECT

In order to confirm the direct relation between the multiple interference effect and the Q factor variations, the entire photonic crystal membrane has been released from the surrounding silicon on buried oxide layer with laser cutting, which allows us to modify the spacing h_{sub} between the PhC slab and the substrate. The entire photonic crystal slab remained suspended on one side via the access wire waveguide. A tungsten tip controlled via piezoactuators was used to push the membrane toward the Si substrate and to control the corresponding spacing h_{sub}. For the different spacing h_{sub}, the cavity spectrum was measured over two decades with a tunable laser, and the Q factor was determined from a Lorentzian fit with an accuracy better than 3%, as shown in Fig. 3(a). The radiated cavity field was simultaneously imaged for each spacing h_{sub} by the 0.95 NA microscope objective [see Fig. 3(c)]. The spacing value h_{sub} was determined from the focusing point of the real space PhC slab image obtained with visible light and crossed checked by comparing the theoretical and experimental far-field spectra.

Figure 3(b) highlights the enhancement and inhibition of the cavity emission for decreasing h_{sub}. The experimental points follow the predicted theoretical variation of Q factor versus h_{sub}. In particular, a clear enhancement of the Q factor is achieved when the PhC membrane is as close as 0.8 μm from the substrate, which agrees with the expected vanishing amplitude of the leaky modes, or equivalently of the transfer function. The corresponding far-field pattern evolves as well according to our theoretical model. The slight asymmetry for $h_{sub} = 0.8$ μm comes from the tilt angle of the PhC slab with regard to the substrate, which is induced by the tip. Note that approaching an object near a mode of a micro cavity is often detrimental for the Q factor due to scattering or absorption of the evanescent contribution of the confined field.[25–27] In contrast, Figs. 3(a) and 3(b) demonstrate here a regime where a planar surface can significantly decrease the mode linewidth of the confined mode, as confirmed also in Fig. 5.

V. ANGULAR SPECTRUM AND SURROUNDING LAYERS OPTIMIZATION FOR HIGH Q MODULATION

The maximum value of the Q factor enhancement based on the multiple interference effect can be optimized by the design of the cavity and of the reflectivity of the surrounding layer. In Fig. 4, we compare the theoretical evolution of the radiative quality factor for a standard L3 cavity and a L3 cavity whose three first holes located on both sides of the line defect have been slightly laterally shifted away from the core by a length of ($0.17a$, $0.07a$, $0.05a$). The angular spectrum of this last cavity [see Fig. 4(a)] is significantly modified compared

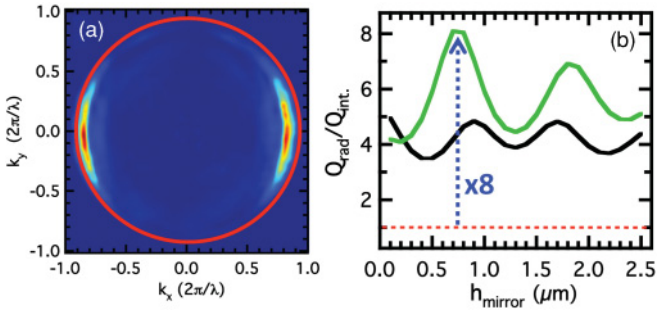

FIG. 4. (Color online) (a) Reconstructed intrinsic intensity angular spectrum of a L3 cavity with shifted holes (red circle: NA = 0.95). (b) Theoretical variations of the radiative quality factor induced by an aluminum reflector for a standard L3 cavity (black line) and a shifted holes L3 cavity (green/gray line), corresponding to the angular spectra in Figs. 2(c) and 4(a), respectively.

to the standard L3 cavity [see Fig. 2(c)] as expected.[14] The vanishing intensity of the field contributions in the middle of the k-space results in a Q factor of 9700 larger than the one of the standard L3. The Q factor is here limited by the in-plane coupling losses.

The role played by the intrinsic nature of the cavity angular spectrum and by the surrounding in the strength of the Q factor enhancement is highlighted in Fig. 4(b). For both types of cavities, a metallic reflector is added above the PhC slab at different distance h_{mirror} [see schematic in Fig. 5(b)]. To model a realistic situation, we have selected as a metal the aluminum whose dielectric constant is $\epsilon_{Al} = -238 + i46.5$ (Ref. 28) at a wavelength of 1.5 μm. When the mirror is added above the PhC membrane, the interference pattern $|t(k_x,k_y)|^2$ is drastically modified. It follows that, in comparison to Fig. 2(d), the radiative quality factor can be enhanced by a factor as large as 5 depending on the spacing h_{mirror} for a standard L3 cavity.

The difference in the evolution of the radiative quality factor between the two types of cavity comes from the difference in their angular spectrum. The specific angular spectrum of the shifted holes cavity that is concentrated in a smaller region of the k-space, results in a Q factor enhancement of 8, larger than for the standard L3 cavity, as well as in a larger Q factor modulation depth.

The optimum cavity in terms of radiation loss suppression and Q factor modulation for a given optical surrounding corresponds to a cavity whose nonvanishing contributions of the radiative far-field spectrum are located at the nodes of the optical environment transfer function. By optimizing both the design of cavity, i.e., its intrinsic angular spectrum, and the transfer function of the optical surrounding, very large Q factor modulation could be achieved in principle. The approach proposed in Ref. 29 to engineer the emission pattern of planar cavity is possibility to achieve higher Q enhancement and modulation.

VI. EXPERIMENTAL Q FACTOR ENHANCEMENT WITH A MOVABLE METALLIC REFLECTOR

In Fig. 5, we investigate a L3 cavity whose three first holes, located on both sides of the line defect, have been slightly laterally shifted by a length of (0.1a, 0.02a, 0.08a) resulting in a Q factor value of 7300 that is mainly limited by the out-of-plane radiation loss. For such a cavity, the insertion coupling was performed in an in-line configuration [see insert of Fig. 5(a)] with an estimated Q_H larger than 40 000. By scanning a metallic mirror on top of the PhC membrane, we experimentally demonstrate in Fig. 5 a larger cavity Q factor enhancement than in Fig. 3. The mirror consists of a 0.9 μm aluminium coating sputtered on a 50 μm thick glass substrate with an area larger than the photonic crystal pattern. In order to minimize the effect of the mechanical fluctuations of the mirror position, the frequency spectrum of the cavity transmission is acquired within less than 1 s. The cavity is excited with a super-continuum light source and the in-line transmission is analyzed with an infrared spectrometer. The quality factor of the infrared spectrometer is limited to $Q_{\text{spetro}} = 14\,000$. Such a procedure that minimizes issues of stability does not allow a very high precision on the Q factor in contrast to the previous spectroscopy implemented in Fig. 3.

The destructive interference effect, that can be viewed as a superposition of the cavity field with its image, is revealed in Fig. 5(a) by a simultaneous 2.6 times increase of the cavity transmission and a 1.5 times increase of the Q factor up to 11 000 $\pm$ 1000. The maximum of the cavity transmission peak and the Q factor are expected to vary concomitantly with an identical amount in order to satisfy the energy conservation. Here the observed discrepancy between the Q factor and the transmission enhancements is mainly due to the spectrometer resolution. Moreover, the difference between the experimental Q factor enhancement and the theoretical one that is expected to be at least larger than 5 [see Fig. 4(b)], is attributed to a residual tilt of the mirror with respect to the 2D membrane, to the nonideal nature of the aluminum mirror and to the limited coupling factor Q_H between the cavity and the W1 access waveguides. Note that the limited resolution of the spectrometer currently hinders the implementation of higher Q factor cavities optimized to induce larger enhancement as for instance the shifted hole L3 cavity discussed in Fig. 4. A next step to improve the dynamical Q factor enhancement based on

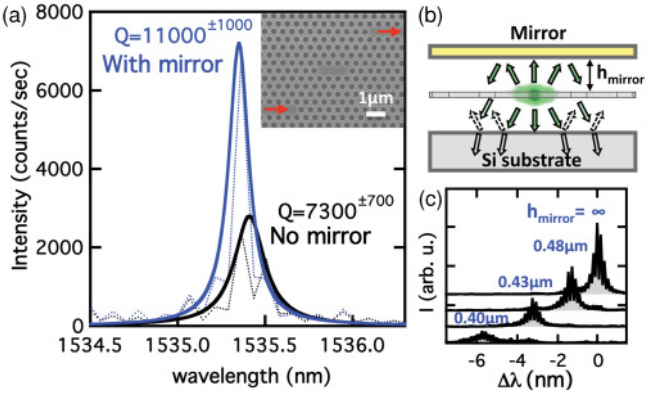

FIG. 5. (Color online) (a) Frequency transmission spectrum envelop of a shifted hole L3 cavity mode with (blue line) and without (dark line) a top metallic mirror. (Insert) PhC pattern. Dotted lines: transmission spectrum. (d) Schematic of the cavity environment. (c) Same as (a) for a standard L3 cavity and a closer mirror position.

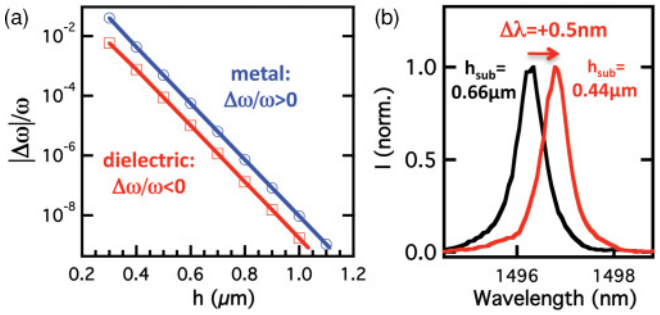

FIG. 6. (Color online) (a) Theoretical frequency shift of a L3 cavity mode induced by a metallic (circles) or a dielectric (squares) planar reflector. (b) Frequency redshift of a type R cavity mode observed when the spacing h_{sub} between a silicon layer and the PhC slab decreases.

the multiple interference effect as well as the precision on the measurement will consist in integrating an actuated reflector directly on-chip above the PhC cavity.

VII. SPECTRAL SHIFTS INDUCED BY PLANAR REFLECTORS

The Q factor enhancement is accompanied by a frequency blueshift of $\Delta\lambda = -0.06$ nm and can be as large as -6 nm when approaching closer the mirror to the cavity [Fig. 5(c)]. Such blueshift originates from the modification of the effective index n_{eff} of the planar photonic crystal membrane layer. The frequency shifts that are induced by approaching a planar layer near the PhC slab and that represents less than 0.5% of the mode frequency, are modeled in Fig. 6. A guided mode calculation based on a standard transfer matrix method predicts a blueshift for a negative dielectric constant metallic layer approaching the membrane, as observed in our paper (see Fig. 5), and a redshift in the case of an approaching dielectric layer, if the index of the surrounding medium equals 1 [see Fig. 6(b)]. In Fig. 6(a), the reflector dielectric constant are $\epsilon_{Al} = -238 + i46.5$ and $\epsilon_{Si} = 12.4$ for the aluminum and the silicon layers, respectively. With the current value of ϵ_{Al}, the observed frequency shift of -0.06 nm in Fig. 4(a) is consistent with $h_{\text{mirror}} = 0.63$ μm.

VIII. CONCLUSION

To conclude, a comprehensive analysis of the angular spectrum of subwavelength confined modes allowed us to experimentally demonstrate active Q factor enhancement based on multiple interference effects. The Q factor enhancement depends on the intrinsic angular spectrum that can be designed as required to match a specific optical surrounding, in particular with photonic crystal cavities. The combination of subwavelength PhC cavities with micro-opto-electromechanical systems[30–34] could contribute to achieve dynamical control of electromagnetic modes. In addition, as the current approach can inhibit radiation losses inherent to highly confined mode, such a combination could as well enhance light matter interaction in dielectric photonic structures.

ACKNOWLEDGMENTS

We would like to thank the ePIXfab platform in IMEC for the fabrication of the PhC samples. This work was supported by the Swiss NCCR-Quantum Photonics, the Swiss National Science Foundation (SNSF) (project 200021-124413), and the COST action MP0702.

[1] E. M. Purcell, Phys. Rev. **69**, 681 (1946).
[2] P. Goy, J. M. Raimond, M. Gross, and S. Haroche, Phys. Rev. Lett. **50**, 1903 (1983).
[3] K. H. Drexhage, in *Progress in Optics*, edited by E. Wolf (North-Holland, Amsterdam, 1974), Vol. 12, p. 165.
[4] B. C. Buchler, T. Kalkbrenner, C. Hettich, and V. Sandoghdar, Phys. Rev. Lett. **95**, 063003 (2005).
[5] R. M. Amos and W. L. Barnes, Phys. Rev. B **55**, 7249 (1997).
[6] E. Yablonovitch, T. J. Gmitter, and R. Bhat, Phys. Rev. Lett. **61**, 2546 (1988).
[7] H. Yokoyama, Opt. Quantum Electron. **24**, S245 (1992).
[8] J. M. Gérard, B. Sermage, B. Gayral, B. Legrand, E. Costard, and V. Thierry-Mieg, Phys. Rev. Lett. **81**, 1110 (1998).
[9] D. Kleppner, Phys. Rev. Lett. **47**, 233 (1981).
[10] E. Yablonovitch, Phys. Rev. Lett. **58**, 2059 (1987).
[11] L. C. Andreani, Phys. Status Solidi B **234**, 139 (2002).
[12] V. Savona, Phys. Rev. B **83**, 085301 (2011).
[13] N. Le Thomas, R. Houdré, M. V. Kotlyar, and T. F. Krauss, Phys. Rev. B **77**, 245323 (2008).
[14] Y. Akahane, T. Asano, B.-S. Song, and S. Noda, Nature **425**, 944 (2003).
[15] E. Kuramochi, M. Notomi, S. Mitsugi, A. Shinya, and T. Tanabe, Appl. Phys. Lett. **88**, 041112 (2006).
[16] N. Le Thomas, R. Houdré, M. V. Kotlyar, D. O'Brien, and T. F. Krauss, J. Opt. Soc. Am. B **24**, 2964 (2007).
[17] W. Lukosz, J. Opt. Soc. Am. **69**, 1495 (1979).
[18] G. Björk, S. Machida, Y. Yamamoto, and K. Igeta, Phys. Rev. A **44**, 669 (1991).
[19] H. Benisty, R. Stanley, and M. Mayer, J. Opt. Soc. Am. A **15**, 1192 (1998).
[20] S. Fan and J. D. Joannopoulos, Phys. Rev. B **65**, 235112 (2002).
[21] S.-H. Kim, S.-K. Kim, and Y.-H. Lee, Phys. Rev. B **73**, 235117 (2006).
[22] L. Ferrier, P. Rojo-Romeo, E. Drouard, X. Letartre, and P. Viktorovitch, Opt. Express **16**, 3136 (2008).
[23] R. Iliew, C. Etrich, T. Pertsch, and F. Lederer, Phys. Rev. B **80**, 035123 (2009).
[24] Y. Tanaka, T. Asano, R. Hatsuta, and S. Noda, Appl. Phys. Lett. **88**, 011112 (2006).
[25] N. Le Thomas, U. Woggon, W. Langbein, and M. V. Artemyev, J. Opt. Soc. Am. B **23**, 2361 (2006).

[26] A. F. Koenderink, M. Kafesaki, B. C. Buchler, and V. Sandoghdar, Phys. Rev. Lett. **95**, 153904 (2005).
[27] W. C. L. Hopman, A. J. F. Hollink, R. M. de Ridder, K. O. van der Werf, V. Subramaniam, and W. Bogaerts, Opt. Express **14**, 8745 (2006).
[28] A. G. Mathewson and H. P. Myers, Phys. Scr. **4**, 291 (1971).
[29] N.-V.-Q. Tran, S. Combrié, and A. De Rossi, Phys. Rev. B **79**, 041101 (2009).
[30] J. S. Harris, IEEE J. Sel. Top. Quantum Electron. **6**, 1145 (2000).
[31] M. Iwamoto and Y. Arakawa, Laser Phys. **16**, 223 (2006).
[32] S. Iwamoto, S. Ishida, Y. Arakawa, M. Tokushima, A. Gomyo, and H. Yamada, Appl. Phys. Lett. **88**, 011104 (2006).
[33] S. Boutami, B. Ben Bakir, J.-L. Leclercq, X. Letartre, C. Seassal, P. Rojo-Romeo, P. Regreny, M. Garrigues, and P. Viktorovitch, IEEE J. Sel. Top. Quantum Electron. **13**, 244 (2007).
[34] M. C. Y. Huang, Y. Zhou, and C. J. Chang-Hasnain, Nat. Photon. **1**, 119 (2007).